medRxiv preprint doi: https://doi.org/10.1101/2021.08.13.21261980; this version posted April 19, 2022. The copyright holder for this preprint (which was not certified by peer review) is the author/funder, who has granted medRxiv a license to display the preprint in perpetuity. It is made available under a CC-BY 4.0 International license .

High gamma activity distinguishes frontal cognitive control regions from adjacent cortical networks

Moataz Assem[1*], Michael G. Hart[2], Pedro Coelho[3], Rafael Romero-Garcia[4], Alexa McDonald[5], Emma Woodberry[5], Robert C. Morris[2], Stephen J. Price[6], John Suckling[4,7,8], Thomas Santarius[2,6,9], John Duncan[1,10], Yaara Erez[11,12,1*]

1 Medical Research Council, Cognition and Brain Sciences Unit, University of Cambridge
2 Department of Neurosurgery, Cambridge University Hospitals NHS Foundation Trust
3 Neurophys Limited
4 Department of Psychiatry, University of Cambridge
5 Department of Neuropsychology, Cambridge University Hospitals NHS Foundation Trust
6 Division of Neurosurgery, Department of Clinical Neurosciences, University of Cambridge.
7 Behavioural and Clinical Neuroscience Institute, University of Cambridge
8 Cambridge and Peterborough NHS Foundation Trust
9 Department of Physiology, Development and Neuroscience, University of Cambridge
10 Department of Experimental Psychology, University of Oxford
11 Faculty of Engineering, Bar-Ilan University, Ramat-Gan, Israel
12 Gonda Multidisciplinary Brain Research Center, Bar-Ilan University, Ramat-Gan, Israel

*Corresponding authors:

Moataz.assem@mrc-cbu.cam.ac.uk

Yaara.Erez@biu.ac.il

NOTE: This preprint reports new research that has not been certified by peer review and should not be used to guide clinical practice.

medRxiv preprint doi: https://doi.org/10.1101/2021.08.13.21261980; this version posted April 19, 2022. The copyright holder for this preprint (which was not certified by peer review) is the author/funder, who has granted medRxiv a license to display the preprint in perpetuity. It is made available under a CC-BY 4.0 International license .

Abstract

Though the lateral frontal cortex is broadly implicated in cognitive control, functional MRI (fMRI) studies suggest fine-grained distinctions within this region. To examine this question electrophysiologically, we placed electrodes on the lateral frontal cortex in patients undergoing awake craniotomy for tumor resection. Patients performed verbal tasks with a manipulation of attentional switching, a canonical control demand. Power in the high gamma range (70-250 Hz) distinguished electrodes based on their location within a high-resolution fMRI network parcellation of the frontal lobe. Electrodes within the canonical fronto-parietal control network showed increased power in the switching condition, a result absent in electrodes within default mode, language, cingulo-opercular and somato-motor networks. High gamma results contrasted with spatially distributed power decreases in the beta range (12-30 Hz). These results confirm the importance of fine-scale functional distinctions within the human frontal lobe, and pave the way for increased precision of functional mapping in tumor surgeries.

medRxiv preprint doi: https://doi.org/10.1101/2021.08.13.21261980; this version posted April 19, 2022. The copyright holder for this preprint (which was not certified by peer review) is the author/funder, who has granted medRxiv a license to display the preprint in perpetuity. It is made available under a CC-BY 4.0 International license .

Introduction

Data from functional magnetic resonance imaging (fMRI) increasingly suggest that the lateral frontal cortex of the human brain is divided into functionally separate regions or networks (1). In the inferior frontal gyrus of the left hemisphere, for example, immediately adjacent regions in single participants are specialized for language or domain-general cognitive control (2). Temporal correlations in resting state data distinguish frontal lobe regions contributing to different whole-brain networks. A recent study using the high-resolution brain parcellation of the human connectome project (HCP) suggests lateral frontal participation in at least five functional networks (3) (**Figure 1b**).

Here we use fMRI fine-scale distinctions of the lateral frontal lobe to examine functional distinctions in intracranially-recorded electrophysiological data. Our focus is on the frontoparietal network (FPN), and its role in executive or cognitive control (4, 5). With electrodes directly placed on the cortical surface, we gathered electrocorticography (ECoG) data in patients undergoing awake brain surgery. To manipulate cognitive control demand we used two tasks, simple counting versus switching between counting and reciting the alphabet (**Figure 1a**). Using the high-resolution HCP network parcellation (3), we assigned each electrode to its nearest resting-state fMRI network. In ECoG data, gamma activity is well established as a measure of local cortical activity (6, 7), and cognitive control tasks have consistently highlighted fMRI activation and gamma power increases in distributed frontal regions (8–11). We predicted that high gamma responses to the switching condition would be localized specifically to regions of the FPN. Often, increases in high gamma activity are associated with decreases in beta band power. Though these two changes may be functionally linked (9), previous data suggest that beta decreases may be more widespread than gamma increases (12). Accordingly, we predicted beta decreases both within and outside the FPN. Our results confirm the importance of fine-scale functional distinctions within the human frontal lobe, and pave the way for increased precision of functional mapping in tumor surgeries.

medRxiv preprint doi: https://doi.org/10.1101/2021.08.13.21261980; this version posted April 19, 2022. The copyright holder for this preprint (which was not certified by peer review) is the author/funder, who has granted medRxiv a license to display the preprint in perpetuity. It is made available under a CC-BY 4.0 International license .

Results

We assigned each of 59 electrodes to its nearest resting-state fMRI network (**Figure 1b; see extended methods**). 36 electrodes were located within the FPN, while 23 were outside this network [8 language (LANG), 5 default-mode (DMN), 4 cingulo-opercular (CON), 6 somato-motor (MOT)]**.** Next we compared spectral power changes between networks for the switch>count contrast. In this contrast, positive values indicate power increases in switch compared to count, while negative values indicate power decreases. We focused on three classical frequency bands: high gamma (HG, 70-250 Hz), low gamma (LG, 30-70 Hz) and beta (12-30 Hz).

First we compared the probability of finding significant electrodes within vs outside of the FPN network. Of the FPN electrodes, 58.3% showed a significant HG increase in the switch>count contrast, compared to 26.1% of non-FPN electrodes (**Figure 1c**). In contrast, the proportions of electrodes showing LG power increases or beta power decreases were similar within and outside the FPN (LG: 22.2% vs. 21.7%, beta: 61.1% vs. 47.8%). Indicating the specificity of the findings to frontal electrodes, all findings replicated after excluding the motor electrodes (HG: 58.3% vs. 35.3%; LG: 22.2% vs. 29.4%; Beta: 61.1% vs. 47.1%). Therefore, only HG increases, but not LG increases nor beta decreases, were more likely within the FPN compared to outside the network.

Figure 1d shows mean percentage power changes in FPN and non-FPN electrodes. HG power increases were significantly stronger in FPN than in non-FPN electrodes **(**unpaired t-test, HG: t_{57}=2.06, p=0.02; p-values are one-tailed due to our directional prediction of gamma increases within the FPN). There was no significant difference between FPN and non-FPN electrodes for LG power increases or beta power decreases (LG: t_{57}=0.99; beta: t_{57}=-0.56). Similarly, all findings replicated after excluding the motor electrodes (HG: t_{51}=2.02, p=0.02; LG: t_{51}=0.73; beta: t_{51}=-0.94). These results confirm that HG power during a demanding task show localized increases specific to frontal regions of the FPN, while beta decreases were widespread.

We further probed whether HG power increases can distinguish between the finer-grained networks. FPN was the only network that showed significant HG power increases (**Figure 1e**; one-sample t-test against zero, FPN t_{35}=2.38, p=0.01

medRxiv preprint doi: https://doi.org/10.1101/2021.08.13.21261980; this version posted April 19, 2022. The copyright holder for this preprint (which was not certified by peer review) is the author/funder, who has granted medRxiv a license to display the preprint in perpetuity. It is made available under a CC-BY 4.0 International license .

one-tailed, DMN t_4=-0.9, LANG t_7=-0.5, CON t_3=1.2, MOT t_5=1.2). FPN also showed significantly stronger HG increases than the DMN (t_{39}=1.93, p=0.03 one-tailed), with a similar trend in the language network (t_{42}=1.49, p=0.07 one-tailed). While other comparisons were not statistically significant, HG increases were also numerically greater in FPN (mean=12.2%) than CON (mean=6.3%) and MOT (mean=2.3%) networks. These results suggest that control-related HG power increases can distinguish the FPN from its surrounding networks.

During the experiment, we had a third experimental condition where patients did not perform any task (rest). Next we assessed the importance of our targeted switch>count contrast, where the conditions are matched in multiple aspects (e.g. speech, counting). Confirming the importance of a targeted contrast, for count>rest the percentage of significant electrodes was similar between FPN and non-FPN electrodes in all three spectral bands (**Figure 1f,** HG increases: 36.1% vs. 35.3%; LG increases: 27.8% vs. 11.8%; beta decreases: 11.1% vs. 11.8%). Neither did the average power modulations differ between FPN and non-FPN electrodes (**Figure 1g;** unpaired t-test, HG: t_{57}=-0.35; LG: t_{57}=0.77; beta t_{57}=1.0). Altogether, these results suggest that HG increases can best distinguish frontal control regions in a well-controlled contrast of demanding versus simple cognitive tasks, in line with recent fMRI findings (11).

medRxiv preprint doi: https://doi.org/10.1101/2021.08.13.21261980; this version posted April 19, 2022. The copyright holder for this preprint (which was not certified by peer review) is the author/funder, who has granted medRxiv a license to display the preprint in perpetuity. It is made available under a CC-BY 4.0 International license .

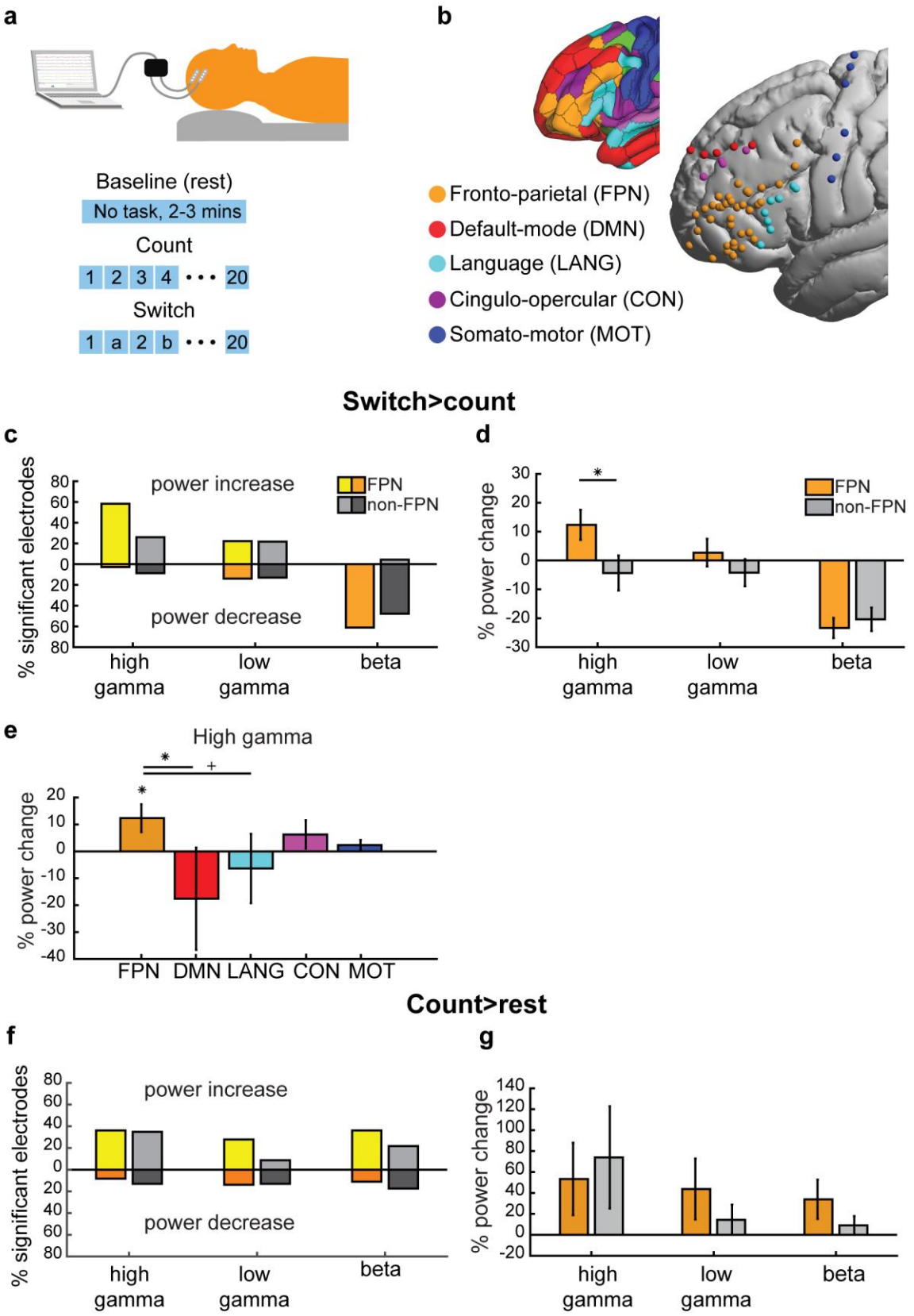

medRxiv preprint doi: https://doi.org/10.1101/2021.08.13.21261980; this version posted April 19, 2022. The copyright holder for this preprint (which was not certified by peer review) is the author/funder, who has granted medRxiv a license to display the preprint in perpetuity. It is made available under a CC-BY 4.0 International license .

Figure 1. (a) Intraoperative setup: Patient is awake during the three experimental conditions and the electrophysiological signals are simultaneously recorded using electrode strips placed directly on the cortical surface. Experimental conditions: rest (no task) and two verbal tasks. The count task involved simple counting from 1 to 20. The switch task involved alternating between numbers and letters. (b) Electrodes colored based on the network label of their nearest vertex. Electrodes on the right hemisphere have been projected onto the left. *Top left inset*: A cortical surface visualization of the 12-network HCP fMRI network parcellation (3). (c) Percentage of electrodes showing significant power modulations out of all electrodes located within (yellow and orange) and outside (light and dark grey) the FPN. Lighter colored bars (above the zero line) show percentage of electrodes with power increases. Darker colored bars (below the zero line) show percentage of electrodes with power decreases. (d) Average power modulations of all electrodes within and outside the FPN for each frequency band for the switch>count contrast. (e) Average power modulations of all electrodes within each network for the switch>count contrast. *$p<0.05$ + $p=0.07$ (f) same as c for the count>rest contrast (g) same as d for the count>rest contrast. Error bars denote SEM.

medRxiv preprint doi: https://doi.org/10.1101/2021.08.13.21261980; this version posted April 19, 2022. The copyright holder for this preprint (which was not certified by peer review) is the author/funder, who has granted medRxiv a license to display the preprint in perpetuity. It is made available under a CC-BY 4.0 International license .

Discussion

While frontal cortex is broadly linked to cognitive control, our ECoG results support fine-grained functional parcellation of this region. We used a canonical demand on executive control, a contrast of cognitive switching versus simple counting (10, 11), and assigned individual electrodes to functional networks from a recent HCP fMRI-based parcellation. In line with our predictions, increases in HG power distinguished the FPN from multiple surrounding regions. Because HG and not LG distinguished frontal control regions, our results support previous suggestions for different physiological origins of high and low gamma (6, 7).

In contrast to localized increases in the HG range, we observed spatially broad decreases in power in the beta band. It has been hypothesized that opposing power changes in these two bands reflect two sides of the same process, a rotated power spectrum around a middle range frequency (9, 13). The current results showed that beta decreases were not necessarily accompanied by gamma increases, supporting recent challenges to this hypothesis (12). Cognitive control models (14) may need extension to explain beta power decreases within but also outside of frontal control regions.

Finally, our findings open the door for high-resolution clinical functional mapping of cognitive control during tumor resection surgeries (15). The link of increased HG power to the FPN establishes a critical anatomo-functional foundation for this approach. Matching the fine scale of regional specializations within frontal cortex, our results suggest that distinct functional regions may be practically mapped in the context of awake tumor surgery.

Materials and Methods

Details on patient recruitment, experimental procedures, MRI and ECoG data acquisition and analysis can be found in the extended methods section.

medRxiv preprint doi: https://doi.org/10.1101/2021.08.13.21261980; this version posted April 19, 2022. The copyright holder for this preprint (which was not certified by peer review) is the author/funder, who has granted medRxiv a license to display the preprint in perpetuity. It is made available under a CC-BY 4.0 International license .

Extended Methods

Patient recruitment

Twenty-one participants were recruited from a pool of patients with glioma undergoing awake craniotomy for tumor resection at the Department of Neurosurgery at Cambridge University Addenbrooke's Hospital (Cambridge, UK). Data from thirteen patients were complete and were included in the study (age range 22-56; 6 males). Data from the remaining eight patients were excluded either due to technical difficulties (n=6; e.g. inability to localize electrodes correctly during surgery) or an inability to perform the tasks (n=2). All study procedures were approved by the East of England - Cambridge Central Research Ethics Committee (REC reference 16/EE/0151). All patients gave written informed consent to participate and were aware that the research would not benefit themselves, or impact their clinical care before, during or after surgery.

Experimental procedures

The patients were familiarized with the tasks during standard pre-operative clinic visits and as part of a pre-operative research-dedicated assessment. During the surgery and following the craniotomy, EEG (electroencephalogram) was recorded from scalp electrodes C3, C4 and Cz referenced to Fz for the purposes of monitoring anaesthetic depth and stimulation-related seizure activity. When the sedation was stopped the EEG evolved from high voltage, semi-rhythmic alpha and theta range components to a continuous trace consisting of the faster beta range frequencies (>13Hz) and low voltage activities in all derivations until the patients were awake. These low voltage beta range rhythms (normal awake activity) persisted during wakefulness and only then did cognitive testing commence. In all patients, testing was performed prior to tumor resection, except for one patient, where testing was performed after partial resection due to clinical considerations. **Figures 1a** illustrates the intraoperative setup and cognitive tasks. During testing, all personnel in the surgical theatre were asked to limit their conversations to minimize disruptions. Patients performed one baseline task and two cognitive tasks.

medRxiv preprint doi: https://doi.org/10.1101/2021.08.13.21261980; this version posted April 19, 2022. The copyright holder for this preprint (which was not certified by peer review) is the author/funder, who has granted medRxiv a license to display the preprint in perpetuity. It is made available under a CC-BY 4.0 International license .

For the baseline task, the patients were asked to stay calm and remain silent for a period of 2-3 minutes (rest). The two cognitive tasks were simple counting (1 to 20; count) and alternate between counting and reciting the alphabet (1, a, 2, b, 3, c, up to 20; switch). Each task condition was repeated for 2-5 trials (median for both = 4 trials) based on each patient's ability and time constraints during the surgery. Trial onset and offset markers were manually recorded on the acquisition system. Trial durations were 20.1±7.4s and 29.4±9.4s for the count and switch conditions, respectively. Most patients were instructed to alternate between trials of the count and switch conditions, though on a few occasions some trials of the same condition were performed in succession. Only correctly performed trials (i.e., no errors in simple or alternate counting) were included in the analysis (e.g., a failed switch trial that was excluded: 1, a, 2, b, 3, b, 4, b, 5, b, 6, b…).

MRI acquisition

MRI data were acquired pre-operatively using a Siemens Magnetom Prisma-fit 3 Tesla MRI scanner and 16-channel receive-only head coil (Siemens AG, Erlangen, Germany). Structural anatomic images were acquired using a T1-weighted (T1w) MPRAGE sequence (FOV = 256 mm x 240 mm x 176 mm; voxel size = 1 mm isotropic; repetition time (TR) = 2300 ms; echo time (TE) = 2.98 ms; flip angle = 9 degrees).

Electrode localization

The extent of craniotomy of all patients was determined by clinical considerations to allow for tumor resection. Based on the craniotomy size and location, one to three electrode strips were placed on the cortical surface in regions judged by the neurosurgeon to be healthy (i.e. macroscopically not containing tumor). Strips placed on the tumor or outside of the frontal and motor cortices were excluded from analysis. Each strip was composed of four electrodes. Two types of strips were used with electrode diameter either 5 mm (MS04R-IP10X-0JH, Ad-Tech, Medical Instruments corporation, WI, USA) or 3 mm (CORTAC 2111-04-081, PMT Corporation, MN, USA). For both strip types, electrode spacing was 10 mm centre to centre.

medRxiv preprint doi: https://doi.org/10.1101/2021.08.13.21261980; this version posted April 19, 2022. The copyright holder for this preprint (which was not certified by peer review) is the author/funder, who has granted medRxiv a license to display the preprint in perpetuity. It is made available under a CC-BY 4.0 International license .

Electrode locations were determined either using (1) an automated method with a probe linked to a stereotactic neuronavigation system (StealthStation® S7® System, Medtronic, Inc, 24 Louisville, CO, USA) or (2) a semi-manual grid method using intraoperative photographs and a grid-like delineation of cortical sulci and gyri. Most electrodes (51/79) were localized using the automated method, but due to occasional technical limitations, 28 electrodes were localized using the grid method. Both methods are detailed below.

(1) Stereotactic neuronavigation: A hand-held probe was placed at the centre of each electrode, automatically registering its physical coordinates, using the neuronavigation system, to the patient's native high resolution preoperative T1w scan. In some cases, coordinate data were available for only two or three out of the four electrodes in each strip. This was due to either time constraints during the surgery or because an electrode was located underneath the skull, excluding probe placement. Each patient's native T1w scan was linearly co-registered with the MNI template volume at 2 mm resolution using FLIRT as implemented in FSL (16) using 12 degrees of freedom (full set affine transformation) and the correlation ratio cost function. The resulting native-to-MNI transformation matrix was then used to convert native electrode coordinates to MNI coordinates.

(2) The grid method: This follows the method described in (17) and (18). (a) Visible major sulci were delineated on the intraoperative photographs: precentral sulcus, sylvian fissure, inferior and superior frontal sulci. Spaces between these sulci were populated by vertical lines (1.5 cm apart) to create a grid-like structure. (b) A grid was created in the same way on a template cortical reconstruction of the MNI volumetric map (reconstructed using the HCP structural preprocessing pipeline 4.0.0; https://github.com/Washington-University/HCPpipelines). (c) MNI coordinates for each electrode were extracted by manually marking its approximate location on the template cortical grid while visualized using the Connectome Workbench v1.4.2 (https://www.humanconnectome.org/software/get-connectome-workbench). As the template cortical reconstruction is co-registered with its MNI volumetric version, it facilitated the automatic transformation of any point marked on the surface back to its MNI volumetric coordinates.

For both localization methods, electrode displacements due to brain shifts following the craniotomy were compensated for by back-projecting the electrode

medRxiv preprint doi: https://doi.org/10.1101/2021.08.13.21261980; this version posted April 19, 2022. The copyright holder for this preprint (which was not certified by peer review) is the author/funder, who has granted medRxiv a license to display the preprint in perpetuity. It is made available under a CC-BY 4.0 International license .

locations onto the cortical surface along the local norm vector (19) as implemented in the fieldtrip (v20160629) protocol for human intracranial data (20).

Electrode network labelling

To relate electrode locations with frontal lobe parcellation identified by fMRI, we used the Cole-Anticevic brain parcellation based on the high resolution data of the human connectome project (HCP) (3). As this parcellation is surface based, we first found the MNI coordinates associated with each surface vertex using the Connectome Workbench (v1.5) function wb_command –surface-coordinates-to-metric (using a group average midthickness surface as it provides the most accurate link between surface and MNI volumetric coordinates). Then we related each electrode to its closest voxel coordinates (shortest Euclidean distance, pdist2 function in MATLAB v2018a) and assigned the electrode the most frequent network label of all voxels within a 5 mm distance.

Electrophysiological data acquisition and analysis

Data were recorded using a 32-channel amplifier (Medtronic Xomed, Jacksonville, FS, USA) sampled at 10 KHz. Potential sources of electrical noise such as the surgical microscope, patient warming blanket, and IV pumps were identified and repositioned to avoid signal contamination. The data were recorded via dedicated channels on the acquisition system and two Butterworth online filters were applied: a high-pass filter at 1 Hz and a low-pass filter at 1500 Hz. A ground needle electrode was connected to the deltoid muscle and the electrodes were referenced to a mid-frontal (Fz) spiral scalp EEG electrode.

Data were analyzed offline using EEGLAB (v13.6.5b) and custom MATLAB scripts. The data were downsampled to 2 kHz then re-referenced using a bipolar scheme to detect any activity changes with the highest spatial resolution as well as to avoid contamination of high frequency signals by scalp muscle artefacts detected by the Fz electrode. The last electrode on the strip was excluded from analysis; i.e. for a four-electrode strip, electrode pairs 1-2, 2-3 and 3-4 were used and assigned to electrode positions 1, 2 and 3, respectively. The location of electrode 4 was discarded. Thus, out of the original 79 electrodes, re-referenced data from 59 were

medRxiv preprint doi: https://doi.org/10.1101/2021.08.13.21261980; this version posted April 19, 2022. The copyright holder for this preprint (which was not certified by peer review) is the author/funder, who has granted medRxiv a license to display the preprint in perpetuity. It is made available under a CC-BY 4.0 International license .

used for further analysis (**Figure 1b**). Out of these 59 electrodes, 41 were on the left hemisphere and 18 on the right. 25 electrodes were placed on the middle frontal gyrus (MFG), 28 on the inferior frontal gyrus (IFG) and 6 on motor cortex.

A notch filter was applied at 50 Hz and its harmonics to remove line noise. Notch filtering was also applied at 79 Hz and its harmonics to remove additional noise observed in the data, likely due to equipment in the surgical theatre. Data were then bandpass filtered into 6 classical frequency bands (delta: 1-4 Hz, theta: 4-8 Hz, alpha: 8-12 Hz, beta: 12-30 Hz, low gamma (LG): 30-70 Hz, high gamma (HG): 70-250 Hz). Instantaneous power of the timeseries was obtained by squaring the absolute amplitude envelope of the Hilbert transformed data.

The power timeseries data were then segmented into separate conditions and trials. Because trial onset and offset markers were manually recorded, 2s from the beginning and end of the rest trial and 1s from each task trial were excluded to account for human reaction time related error. For the switch trials, a further 3s from the beginning of each trial was excluded to discard the initial easy phase of this task (e.g., 1, a, 2, b, 3, c). One power value for each condition was obtained by concatenating its data across trials and averaging across time points. For each pair of conditions (switch>count, count>rest), the percentage of signal change was computed as: [(power in condition 1/power in condition 2) – 1] * 100.

For each electrode, a permutation testing approach was used to statistically compare power change across each pair of conditions. For each electrode, the instantaneous power timeseries of all task trials from both conditions were concatenated serially to form a loop in the same order in which they were conducted. To close the loop, the end of the last trial was joined to the beginning of the first trial. All trial onset/offset markers were then shifted using the same jitter (randomly generated for each permutation), allowing them to “rotate” along the data loop. This rotation approach was used to generate surrogate power data while preserving trial lengths and the temporal correlations in the data. After the rotation, we computed the mean power (for each condition) and power ratio (across conditions) based on the new trial markers. Applying this rotation approach on the timeseries of the power rather than the raw data ensured that there were no artefacts in the form of sudden power changes at the points of trials concatenation. This process was repeated 100,000 times to create a surrogate distribution against which

medRxiv preprint doi: https://doi.org/10.1101/2021.08.13.21261980; this version posted April 19, 2022. The copyright holder for this preprint (which was not certified by peer review) is the author/funder, who has granted medRxiv a license to display the preprint in perpetuity. It is made available under a CC-BY 4.0 International license .

two-tailed statistical significance was calculated (percentile ranks 97.5 and 2.5) for each electrode.

Acknowledgments

The Royal Society provided financial support in the form of a Royal Society Dorothy Hodgkin Research Fellowship to YE (DH130100). Cambridge Commonwealth European and International Trust provided financial support in the form of a Yousef Jameel scholarship to MA. Guarantors of Brain provided financial support in the form of a Post-Doctoral Fellowship award to RRG. The National Institute for Health Research (NIHR, UK) provided financial support in the form of a Clinician Scientist Award 35 to SJP (ref: NIHR/CS/009/011). The Brain Tumour Charity provided financial support in the form of a grant award to MGH, TS and YE (ref: RG86218). J.D was funded by a Medical Research Council grant (MC_UU_00005/6). All the sponsors had no role in the design or conduct of this research. We thank Mallory Owen for help with administering and analyzing neuropsychological tests of the patients.

Data Availability

Due to clinical ethical considerations and in accordance with the ethics approval for the study by the East of England - Cambridge Central Research Ethics Committee (REC reference 16/EE/0151), the data cannot be shared or become publicly available.

medRxiv preprint doi: https://doi.org/10.1101/2021.08.13.21261980; this version posted April 19, 2022. The copyright holder for this preprint (which was not certified by peer review) is the author/funder, who has granted medRxiv a license to display the preprint in perpetuity. It is made available under a CC-BY 4.0 International license .

References

1. M. F. Glasser, *et al.*, A multi-modal parcellation of human cerebral cortex. *Nature* **536**, 171–178 (2016).
2. E. Fedorenko, J. Duncan, N. Kanwisher, Language-selective and domain-general regions lie side by side within Broca's area. *Curr. Biol.* **22**, 2059–2062 (2012).
3. J. L. Ji, *et al.*, Mapping the human brain's cortical-subcortical functional network organization. *Neuroimage* **185**, 35–57 (2019).
4. J. Duncan, The multiple-demand (MD) system of the primate brain: mental programs for intelligent behaviour. *Trends Cogn. Sci.* **14**, 172–179 (2010).
5. M. W. Cole, *et al.*, Multi-task connectivity reveals flexible hubs for adaptive task control. *Nat. Neurosci.* **16**, 1348–1355 (2013).
6. J.-P. Lachaux, N. Axmacher, F. Mormann, E. Halgren, N. E. Crone, High-frequency neural activity and human cognition: Past, present and possible future of intracranial EEG research. *Prog. Neurobiol.* **98**, 279–301 (2012).
7. N. E. Crone, A. Sinai, A. Korzeniewska, "High-frequency gamma oscillations and human brain mapping with electrocorticography" in *Progress in Brain Research*, (2006), pp. 275–295.
8. M. Haller, *et al.*, Persistent neuronal activity in human prefrontal cortex links perception and action. *Nat. Hum. Behav.* **2**, 80–91 (2018).
9. R. F. Helfrich, R. T. Knight, Oscillatory Dynamics of Prefrontal Cognitive Control. *Trends Cogn. Sci.* **20**, 916–930 (2016).
10. E. Fedorenko, J. Duncan, N. Kanwisher, Broad domain generality in focal regions of frontal and parietal cortex. *Proc. Natl. Acad. Sci.* **110**, 16616–16621 (2013).
11. M. Assem, M. F. Glasser, D. C. Van Essen, J. Duncan, A Domain-General Cognitive Core Defined in Multimodally Parcellated Human Cortex. *Cereb. Cortex* **30**, 4361–4380 (2020).
12. M.-C. Fellner, *et al.*, Spectral fingerprints or spectral tilt? Evidence for distinct oscillatory signatures of memory formation. *PLOS Biol.* **17**, e3000403 (2019).
13. E. Podvalny, *et al.*, A unifying principle underlying the extracellular field potential spectral responses in the human cortex. *J. Neurophysiol.* **114**, 505–519 (2015).
14. E. K. Miller, M. Lundqvist, A. M. Bastos, Working Memory 2.0. *Neuron* **100**, 463–475 (2018).
15. Y. Erez, *et al.*, Intraoperative mapping of executive function using electrocorticography for patients with low-grade gliomas. *Acta Neurochir. (Wien).* **163**, 1299–1309 (2021).

medRxiv preprint doi: https://doi.org/10.1101/2021.08.13.21261980; this version posted April 19, 2022. The copyright holder for this preprint (which was not certified by peer review) is the author/funder, who has granted medRxiv a license to display the preprint in perpetuity. It is made available under a CC-BY 4.0 International license .

16. M. Jenkinson, C. F. Beckmann, T. E. J. Behrens, M. W. Woolrich, S. M. Smith, FSL. *Neuroimage* **62**, 782–790 (2012).

17. V. Havas, A. Gabarrós, X. Rifa-ros, G. Plans, Brain & Language Electrical stimulation mapping of nouns and verbs in Broca ' s area. **146**, 53–63 (2015).

18. G. Ojemann, J. Ojemann, E. Lettich, M. Berger, Cortical language localization in left, dominant hemisphere. *J. Neurosurg.* **71**, 316–326 (1989).

19. D. Hermes, K. J. Miller, H. J. Noordmans, M. J. Vansteensel, N. F. Ramsey, Automated electrocorticographic electrode localization on individually rendered brain surfaces. *J. Neurosci. Methods* **185**, 293–298 (2010).

20. A. Stolk, *et al.*, Integrated analysis of anatomical and electrophysiological human intracranial data. *Nat. Protoc.* **13**, 1699–1723 (2018).